Title

Transition of a Hyperpycnal Flow Into a Saline Turbidity Current Due to Differential Diffusivities

Journal

Geophysical Research Letters, 45(21)

ISSN

0094-8276

Authors

Zhao, Liang
Ouillon, Raphael
Vowinckel, Bernhard
et al.

Publication Date

2018-11-16

DOI

10.1029/2018gl080150

Peer reviewed

Geophysical Research Letters

RESEARCH LETTER
10.1029/2018GL080150

Transition of a Hyperpycnal Flow Into a Saline Turbidity Current due to Differential Diffusivities

Liang Zhao[1,2], Raphael Ouillon[2], Bernhard Vowinckel[2], Eckart Meiburg[2], Benjamin Kneller[3], and Zhiguo He[1]

[1]Ocean College, Zhejiang University, Hangzhou, China, [2]Department of Mechanical Engineering, University of California, Santa Barbara, CA, USA, [3]School of Geosciences, University of Aberdeen, Kings College, Aberdeen, UK

Abstract We provide a new perspective on the transition of hyperpycnal flows into saline turbidity currents, which permits longer runout lengths than might be otherwise expected. This mechanism relies on the differential turbulent diffusion of salt and sediment, and in contrast to ambient saltwater entrainment it enables the salinification of the freshwater current without diluting the sediment concentration field by a corresponding amount. The freshness-to-sediment ratio is introduced in order to quantify the transition process. The results of high-resolution simulations provide estimates for the transition distance of hyperpycnal model flows into saline turbidity currents.

Plain Language Summary In some near-coastal areas of the world's oceans, sediment-rich rivers trigger so-called hyperpycnal currents, which are currents composed of river-derived freshwater and sediment that propagate along the seafloor. In general, one may expect such currents to have a short runout length, since sediment deposition will reduce their density until they loft from the seafloor. There is evidence, however, that in some settings hyperpycnal currents can have much larger runout lengths than expected. Here we propose a novel perspective on such large runout lengths, by showing that differential diffusivities can enable the hyperpycnal flow to transition into a saline turbidity current. This mechanism relies on the fact that salt and sediment diffuse at different rates, so that the freshwater current can become salinified without diluting its sediment concentration field.

Key Points:
- Differential diffusion provides a new perspective on the transition of hyperpycnal flows into saline turbidity currents
- Differential diffusion of salt and sediment can render the freshwater current salty, without strongly diluting the sediment
- Transition distance estimates are provided for hyperpycnal model flows

Correspondence to:
E. Meiburg,
meiburg@engineering.ucsb.edu

Citation:
Zhao, L., Ouillon, R., Vowinckel, B., Meiburg, E., Kneller, B., & He, Z. (2018). Transition of a hyperpycnal flow into a saline turbidity current due to differential diffusivities. *Geophysical Research Letters*, *45*. https://doi.org/10.1029/2018GL080150

Received 24 AUG 2018
Accepted 29 OCT 2018
Accepted article online 1 NOV 2018

1. Introduction

Gravity drives the redistribution of material on the Earth's surface from the continents to the deep oceans, often with one or more staging areas on its way. Within the marine environment, downslope transport from the shoreline or shallow marine environment takes the form of sediment gravity flows, that is, flowing mixtures of sediment and water (Talling et al., 2012). Most important for the long-range transport of sediment are turbidity currents, which include flows ranging from dilute laminar or turbulent muddy suspensions to concentrated flows of sand and water (McCave & Jones, 1988; Meiburg & Kneller, 2010; Mulder & Alexander, 2001). Initiation of turbidity currents may occur in a variety of ways (see the review by Talling et al., 2013), but in certain settings, the most important triggering mechanism is by hyperpycnal flow (Mulder et al., 2003; Talling, 2014), in which the suspended sediment load of a river in flood may be sufficiently high that the discharge of freshwater and sediment into the ocean is denser than seawater (Mulder & Syvitski, 1995; Nakajima, 2006), and thus generates a turbid underflow. This is most common in marine settings adjacent to mountainous regions with rapid uplift, a monsoonal typhoon-dominated climate and where continental shelves are narrow or absent, such as Taiwan (Carter et al., 2012).

While the long runout length of traditional, saline turbidity currents remains an active research area (Kneller et al., 2016; Luchi et al., 2018), the situation is somewhat different for hyperpycnal freshwater flows. These can be sustained only so long as the bulk density of the sediment-freshwater mixture is higher than that of the ambient seawater and the flow remains negatively buoyant. As deposition proceeds, the bulk density decreases until the buoyancy becomes neutral, the gravitational force on the current falls to zero and the current ceases to move forward. At this point the turbulence maintaining the particles in suspension decays rapidly and the suspension collapses, triggering a rapid decrease in density and buoyancy reversal. The depositional limit of coarser-grained material that has fallen from suspension tends to be abrupt, whereas finer

material is carried aloft with the lighter fluid that constitutes the now positively buoyant flow (Gladstone & Pritchard, 2010). This lofting flow may reach the free surface or spread along an interface of equal density within a stratified ambient, to produce a more widely dispersed fall-out deposit.

A situation in which deposition and subsequent lofting are less likely to occur is where hyperpycnal flows discharge into submarine canyons such as those off the southeast coast of Taiwan. Submarine cable breaks associated with typhoon-triggered hyperpycnal flows demonstrate that such flows may persist for hundreds of kilometers down the continental slope (Carter et al., 2012; Gavey et al., 2017). One possible mechanism to explain this tremendous runout distance is by self-acceleration (Blanchette et al., 2005; Hu et al., 2015; Parker et al., 1986). Under such conditions, instead of depositing sediments on the canyon floor, the downslope hyperpycnal flow erodes additional sediment from the bed and thus increases its bulk density and runout length.

As an alternative explanation for the observed increased runout length of hyperpycnal flows, several authors have proposed that the river-generated fresh water current could develop into a robust and long-runout turbidity current by entraining saline ambient water (Mulder et al., 2003; Nakajima, 2006). A number of laboratory experiments (Gladstone & Pritchard, 2010; Sparks et al., 1993; Steel et al., 2017; Sutherland et al., 2018) indeed demonstrate that instabilities on the surface of a freshwater hyperpycnal current entrain ambient saline fluid by engulfing patches of salt water that subsequently mix with the current fluid via diffusion at the smallest scales. However, while the entrainment of saline ambient without particles increases the salinity of the interstitial fluid, it simultaneously dilutes the sediment concentration field. As a net result, the bulk density of the current is reduced, so that entrainment of ambient salt water by itself cannot explain the runout length of hyperpycnal flows.

The present investigation explores an alternative scenario for the transition of a hyperpycnal flow into a saline turbidity current. This scenario is based on differences in the effective diffusivities of salt and sediment. At the smallest scales their rates of diffusion are governed by the molecular diffusivity of salt, and the corresponding hydrodynamic diffusivity of particles. While the molecular diffusivity of salt in water has a well-established value of approximately $1.6 \times 10^{-9} m^2/s$, the equivalent small-scale diffusivity of particles due to their hydrodynamic interaction depends on their size, density, and settling velocity (Segre et al., 2001). For an introduction into the hydrodynamic diffusion of non-Brownian particles, we refer the reader to Davis (1996). These small-scale diffusivities of salt and sediment need to be carefully distinguished from their effective diffusivities which result from the interaction of turbulent entrainment and molecular diffusion. These effective diffusivities govern the large-scale scalar transport, and they depend on the flow conditions such as the Reynolds number.

The issue of differential turbulent diffusivities of salt and heat has attracted some attention in the past, primarily in the context of internal waves and turbulent shear flows. Hebert and Ruddick (2003) focus on the case of breaking internal waves. Rather than salt and heat, they analyze the turbulent diffusivity of two different dyes with different molecular diffusivities. In almost all of their experiments these dyes function as passive tracers, while the density difference is provided by salt. For sufficiently large buoyancy Reynolds numbers, the authors observe turbulent diffusivity ratios of the two dyes near one. Smyth et al. (2005) analyze the turbulent diffusivity ratio of heat and salt in breaking Kelvin-Helmholtz waves of stably stratified flows. However, they consider only cases in which both salt and temperature are stably stratified, so that double-diffusive effects are absent. Again, they observe turbulent diffusivity ratios near unity for large buoyancy Reynolds numbers. Similarly, double-diffusive effects are absent from the stratified DNS simulations of Merryfield (2005), who finds that the turbulent diffusivity ratio approaches one as the buoyancy frequency increases. To our knowledge, the issue of differential turbulent diffusivities in double-diffusively unstable shear flows has not yet been investigated.

Burns and Meiburg (2015) conduct DNS simulations to analyze the double-diffusive instability that develops when fresh water containing sediment is placed above saltwater, in the absence of externally imposed shear. They model the sediment phase as a settling scalar whose molecular diffusivity is 25 times *smaller* than that of the salt. Perhaps somewhat surprisingly, they find that the turbulent diffusivity of the sediment is *larger* than that of salt, by a factor of approximately two. We remark that in this setup, where the fluid is at rest initially everywhere, the increase in the potential energy of the upward spreading salinity has to be provided by the potential energy loss of the downward spreading sediment. Since the base state density contribution of the salinity exceeds that of the sediment, energetic arguments dictate that the effective diffusivity of the sediment has to be larger than that of the salinity. A corresponding argument suggests that if we place sediment-laden

fresh water below salt water, the effective diffusivity of salt must exceed that of sediment, so that the lower layer gains salinity more quickly than it loses sediment. Note, however, that this argument does not necessarily transfer to double-diffusively unstable shear flows, where an additional source of energy is provided by the shear.

The above investigations indicate that in high Reynolds number, double-diffusively stable shear flows the turbulent diffusivity ratio tends toward unity. On the other hand, double-diffusive instability without shear favors turbulent diffusivity ratios substantially different from one. The precise value will depend on the individual molecular diffusivities, on the density ratio, as well as on the settling velocity if one of the phases is particulate. The effective diffusivities of heat and salt in double-diffusive turbidity currents may hence differ substantially, which motivates the present investigation. A simple, semianalytic model for double-diffusively unstable gravity currents developed by McDougall (1985) predicts that the density of the gravity current should increase as a result of double diffusion, a finding that is consistent with the recent DNS investigation of Konopliv and Meiburg (2016). This suggests that in hyperpycnal currents containing freshwater and sediment, the double-diffusive mechanism will indeed tend to raise the current density by increasing its salinity, which should favor the transition of the hyperpycnal flow into a saline, relatively undiluted turbidity current that can propagate over much longer distances. Additionally, sediment can remain in suspension for longer times as its density difference with the increasingly saline interstitial fluid is reduced.

In the following we will employ high-resolution, two-dimensional direct numerical simulations in order to explore how the transition of a fresh particle-laden gravity current into a saline turbidity current can result from the differential diffusivities of salt and sediment at the freshwater/salt water interface. The ability of differential diffusion to generate such a transition over a range of parameters will be demonstrated, and we will discuss scaling considerations for estimating the transition time and distance.

2. Mathematical Modeling

The initial setup for generating a lock-exchange hyperpycnal flow propagating into a saline ambient is presented in Figure 1. Quantities in their dimensional form are denoted by the ˆ-symbol, while variables without this symbol are dimensionless. The density of the initial freshwater-sediment mixture is $\hat{\rho}_L$, while the ambient salt water has the lower density $\hat{\rho}_R$. A vertical gate initially separates the fluids. Once the gate is removed, the freshwater-sediment mixture forms a bottom-propagating hyperpycnal current that interacts with the ambient salt water. At the most fundamental level, there are two mechanisms by which the sediment can become embedded in salty water: (1) salinity can diffuse across the current/ambient interface, and (2) in regions where fresh water and sediment are located above clear salt water, particles can settle across the fresh water/salt water interface into the saline ambient. The current investigation focuses on the former mechanism, and hence we assume a vanishing particle settling velocity. This also prevents the loss of sediment by deposition onto the bed.

2.1. Governing Equations

We employ the Navier-Stokes equations for an incompressible flow in their Boussinesq approximation. We furthermore assume that the sediments form a dilute suspension with relatively low volume fraction (<1%) such that particle-particle interactions can be neglected, and that the particles are sufficiently small to be considered noninertial (Necker et al., 2002). This allows us to employ advection-diffusion equations for the transport of salinity and sediment. In index notation, we obtain

$$\frac{\partial \hat{u}_j}{\partial \hat{x}_j} = 0, \tag{1}$$

$$\frac{\partial \hat{u}_i}{\partial \hat{t}} + \hat{u}_j \frac{\partial \hat{u}_i}{\partial \hat{x}_j} = -\frac{1}{\hat{\rho}_0}\frac{\partial \hat{p}}{\partial \hat{x}_i} + \hat{\nu}\frac{\partial^2 \hat{u}_i}{\partial \hat{x}_j \partial \hat{x}_j} + \frac{\hat{\rho}-\hat{\rho}_0}{\hat{\rho}_0}\hat{g}e_i^g, \tag{2}$$

$$\frac{\partial \hat{c}}{\partial \hat{t}} + \hat{u}_j \frac{\partial \hat{c}}{\partial \hat{x}_j} = \hat{\kappa}_c \frac{\partial^2 \hat{c}}{\partial \hat{x}_j \partial \hat{x}_j}, \tag{3}$$

$$\frac{\partial \hat{s}}{\partial \hat{t}} + \hat{u}_j \frac{\partial \hat{s}}{\partial \hat{x}_j} = \hat{\kappa}_s \frac{\partial^2 \hat{s}}{\partial \hat{x}_j \partial \hat{x}_j}. \tag{4}$$

Here $\hat{u}$ denotes the velocity of the fluid-particle mixture, with the subscripts i, j indicating the x or y direction, respectively. $\hat{\rho}$ and $\hat{\rho}_0$ represent the local density and the density of fresh water, respectively, $\hat{t}$ is time, and $\hat{\nu}$

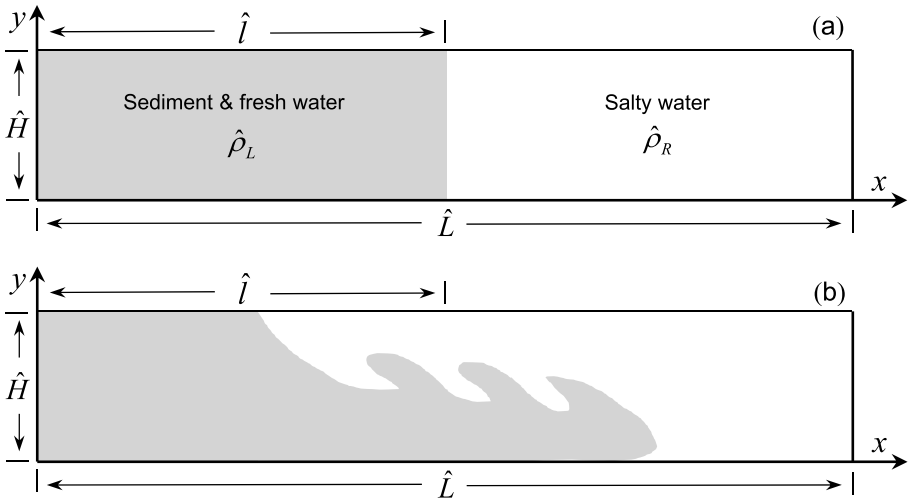

Figure 1. A lock-exchange, sediment-laden hyperpycnal current propagating into salty ambient water. (a) Initial condition; (b) intermediate stage of the flow.

denotes the kinematic viscosity. $\hat{g}$ indicates the gravitational acceleration, with $e_i^g = (0, -1)$ being the unit normal vector in the direction of gravity. $\hat{c}$ denotes the sediment concentration with molecular diffusivity $\hat{\kappa}_c$, while $\hat{s}$ indicates the salinity with molecular diffusivity $\hat{\kappa}_s$. Since we neglect the settling motion of the sediment, the above equations are equivalent to those describing a heat/salt system.

We assume a linear equation of state for the density as a function of salinity and sediment concentration such that

$$\hat{\rho} = \hat{\rho}_0 + \alpha\hat{c} + \beta\hat{s}, \tag{5}$$

where α and β denote the respective density expansion coefficients. The densities of the initial sediment-laden water and saline water can be expressed by

$$\hat{\rho}_L = \hat{\rho}_0 + \alpha\hat{c}_0 \tag{6}$$

and

$$\hat{\rho}_R = \hat{\rho}_0 + \beta\hat{s}_0, \tag{7}$$

with $\hat{c}_0$ and $\hat{s}_0$ indicating the initial sediment concentration and salinity values, respectively. The equations are made nondimensional by introducing the reference scales

$$\hat{\mathbf{x}} \to \mathcal{L}\mathbf{x}, \tag{8}$$

$$\hat{\mathbf{u}} \to \mathcal{U}\mathbf{u}, \tag{9}$$

$$\hat{t} \to \frac{\mathcal{L}}{\mathcal{U}}t, \tag{10}$$

$$\hat{p} \to \hat{\rho}_0\mathcal{U}^2 p, \tag{11}$$

$$\hat{c} \to \mathcal{C}c, \tag{12}$$

$$\hat{s} \to \mathcal{S}s, \tag{13}$$

where $\mathcal{L} = \hat{H}/2$ is the channel half-height, $\mathcal{U} = \hat{u}_b = \sqrt{\hat{g}\hat{H}(\hat{\rho}_L - \hat{\rho}_R)/(2\hat{\rho}_0)}$ is the buoyancy velocity, and $\mathcal{C} = \hat{c}_0$ and $\mathcal{S} = \hat{s}_0$ are the sediment concentration and salinity scales, respectively. By substituting equations (5), (6), and (7) into equations (1)–(4) and adopting these characteristic scales, we obtain the nondimensional governing equations

$$\frac{\partial u_j}{\partial x_j} = 0, \tag{14}$$

$$\frac{\partial u_i}{\partial t} + u_j\frac{\partial u_i}{\partial x_j} = -\frac{\partial p}{\partial x_i} + \frac{1}{Re}\frac{\partial^2 u_i}{\partial x_j \partial x_j} + \left(R_L c + R_R s\right) e_i^g, \tag{15}$$

$$\frac{\partial c}{\partial t} + u_j \frac{\partial c}{\partial x_j} = \frac{1}{Pe_c} \frac{\partial^2 c}{\partial x_j \partial x_j}, \tag{16}$$

$$\frac{\partial s}{\partial t} + u_j \frac{\partial s}{\partial x_j} = \frac{1}{Pe_s} \frac{\partial^2 s}{\partial x_j \partial x_j}. \tag{17}$$

The Reynolds number Re is defined as

$$Re = \frac{\hat{u}_b \hat{H}}{2\hat{\nu}}, \tag{18}$$

while the Peclet numbers of sediment and salt take the form

$$Pe_c = ReSc_c, Pe_s = ReSc_s, \tag{19}$$

where the respective turbulent Schmidt numbers of sediment and salt are given by

$$Sc_c = \frac{\hat{\nu}}{\hat{\kappa}_c}, Sc_s = \frac{\hat{\nu}}{\hat{\kappa}_s}. \tag{20}$$

Two dimensionless density parameters appear in the form

$$R_L = \frac{\hat{\rho}_L - \hat{\rho}_0}{\hat{\rho}_L - \hat{\rho}_R}, \qquad R_R = \frac{\hat{\rho}_R - \hat{\rho}_0}{\hat{\rho}_L - \hat{\rho}_R}. \tag{21}$$

The ratio τ of the turbulent salinity and sediment diffusivities is denoted as $\tau = Pe_c/Pe_s = \kappa_s/\kappa_c$.

2.2. Boundary Conditions, Initial Conditions, and Numerical Approach

We impose no-slip boundary conditions along the bottom and side walls, and a free-slip condition along the top wall in order to emulate a free surface. No-flux conditions are implemented along all walls for the salinity and sediment concentration fields. The uniform mesh size is 0.004 in all simulations, which we found to be sufficiently small for the simulations to be well resolved.

In all of the simulations to be discussed in the following, $L = 50$, $l = 20$, $H = 2$, and $\hat{\rho}_R = 1{,}010$ kg/m^3. An initial sediment volume fraction of 1% is assumed, with a particle density of 2,650 kg/m^3. With a fresh water density of 1,000 kg/m^3, this results in $\hat{\rho}_L = 1{,}016.5$ kg/m^3, with $\alpha = 2.5835$, and $\beta = 1.5835$.

To calculate the evolution of the flow field, we employ our incompressible Navier-Stokes solver *PARTIES* (Biegert, Vowinckel, & Meiburg, 2017; Biegert, Vowinckel, Ouillon, et al., 2017), which uses second order central finite differences to discretize the viscous terms, along with a second order upwind scheme for the advection terms. A third order low-storage Runge-Kutta method is used to advance the flow field in time. The pressure-projection method is implemented, based on a direct fast Fourier transform solver for the resulting Poisson equation at each Runge-Kutta substep.

3. Analysis of the Transition Process

In order to document the transition process from a hyperpycnal current to a saline turbidity current, we analyze the temporal evolution of several diagnostic quantities, as explained in the following. At the most basic level, we define the current front location as the furthest downstream point (x_f, y_f) for which the sediment concentration is larger than a threshold concentration value, that is, $c > c_t$. Throughout the present study, we choose $c_t = 0.5$. In addition, we track the temporal evolution of various properties of the frontal region of the current. Toward this end, we compute the average value of a given quantity q in the frontal region as

$$\langle q \rangle_{fr} = \frac{\int_{\Omega_{fr}} \gamma q dV}{\int_{\Omega_{fr}} \gamma dV}, \tag{22}$$

where $\gamma = \begin{cases} 1 & \text{if} c > c_t \\ 0 & \text{otherwise} \end{cases}$, and $\Omega_{fr} = \begin{cases} \Omega(x_f - L_t < x < x_f) & \text{if } x_f > l + L_t \\ \Omega(l < x < x_f) & \text{otherwise} \end{cases}$. Here Ω denotes the whole computational domain; l is the length between the left wall and the gate; and L_t is a length chosen to define the extent of the frontal region. We generally set $L_t = 2H$. Several choices of q are useful in terms of shedding light on the transition process, such as the sediment concentration c, the salinity s, and the density $\rho = R_L c + R_R s$. In addition, we will also focus especially on the product cs in this context, as well as on the ratio $\xi = (1 - s)/c$.

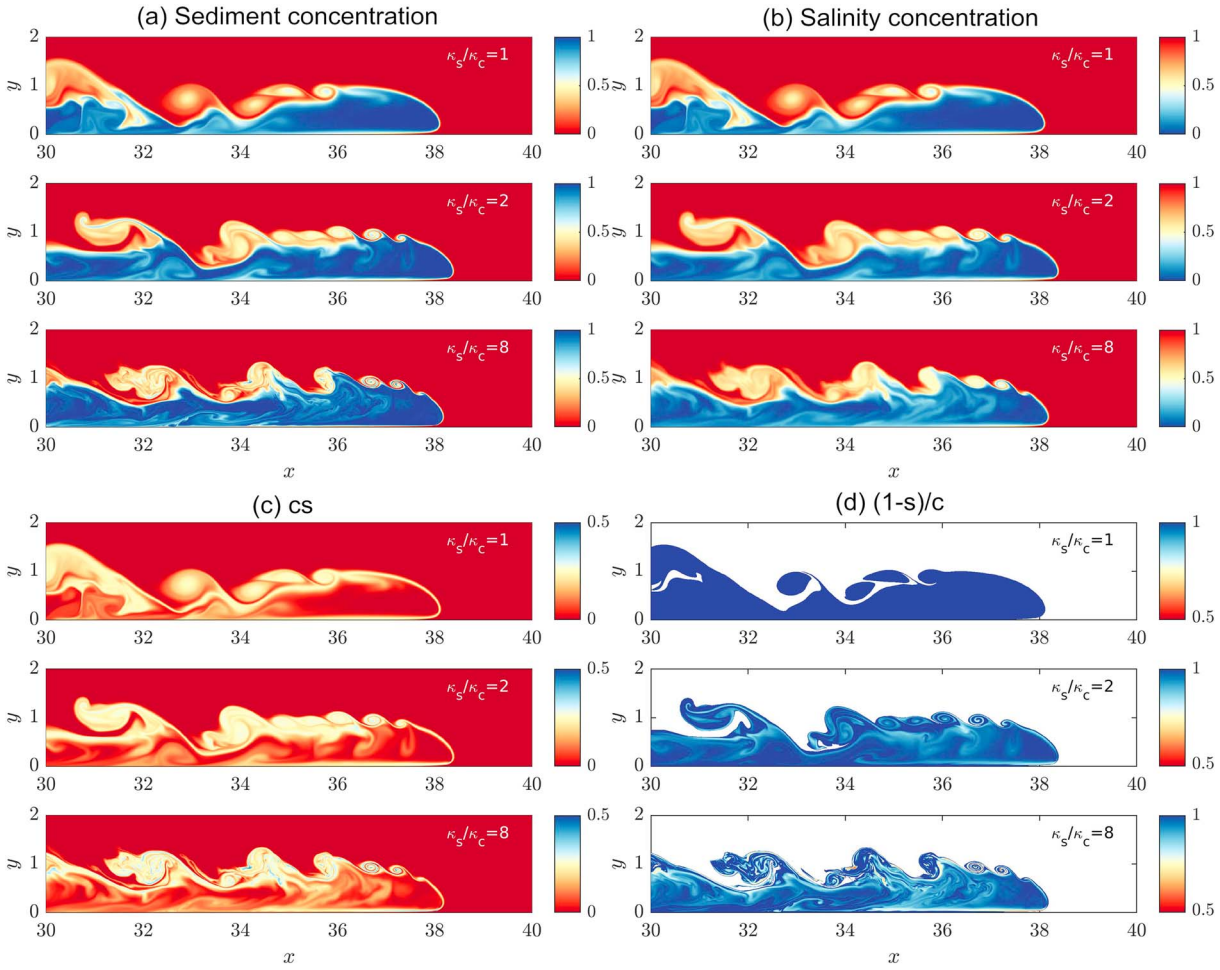

Figure 2. Hyperpycnal current propagating into a saline ambient. Shown are various flow quantities at time $t = 30$, for the three diffusivity ratios $\tau = \kappa_s/\kappa_c = 1$, 2, and 8. (a) Sediment concentration field, (b) salinity field, (c) *cs*, and (d) freshness-to-sediment ratio $\xi = (1 - s)/c$. As τ increases, the salinity of the current increases rapidly without a corresponding loss of sediment, so that the current transitions from a hyperpycnal flow to a saline turbidity current.

The quantity *cs* reflects the simultaneous presence of salinity and sediment in a fluid element. Initially $cs = 0$ everywhere, and the subsequent increase of *cs* with time reflects the extent to which the interstitial fluid is becoming saline. However, any amount of diffusion of either salinity or sediment will result in nonzero values of *cs*, so that this quantity by itself does not provide any insight into the effects of *differential* diffusivities of salinity and sediment. Toward this end, the quantity ξ is more informative for analyzing the transition of a hyperpycnal current to a saline turbidity current. With *s* being the salinity, $(1 - s)$ can be interpreted as the *absence of salinity*, or as the *freshness* of the fluid. If the diffusivities of salt and sediment are identical, $(1 - s)$ and *c* are governed by the same transport equations, initial and boundary conditions, so that throughout the evolution of the flow $\xi = 1$ where sediment is present. Any deviation from $\xi = 1$ therefore reflects the effects of differential diffusivities. With salinity being the faster diffuser, we expect $\langle\xi\rangle_{fr}$ in the current to decrease with time. Small values of $\langle\xi\rangle_{fr}$ will indicate that the interstitial fluid has become largely saline.

4. Transition From Hyperpycnal Flow to Saline Turbidity Current

The frames of Figure 2 display the *c*-, *s*-, *cs*-, and ξ-fields at time $t = 30$, for diffusivity ratios $\tau = \kappa_s/\kappa_c$ of 1, 2, and 8. We set $Re = 3{,}000$, which corresponds to a weakly turbulent laboratory-scale current. To keep the computational effort manageable, we keep the Peclet number for the fast diffuser (*salt*) fixed at $Pe_s = Re = 3{,}000$, while we consider slow diffusers (*sediment*) with Peclet numbers $Pe_c = 3{,}000$, 6,000, and 24,000, so that the molecular diffusivity is $O(10^3)$ larger than for real flows. We hence need to keep in mind that the scaling results to be discussed in the following, especially regarding the transition time, are obtained for laboratory-scale currents with enhanced molecular diffusivities.

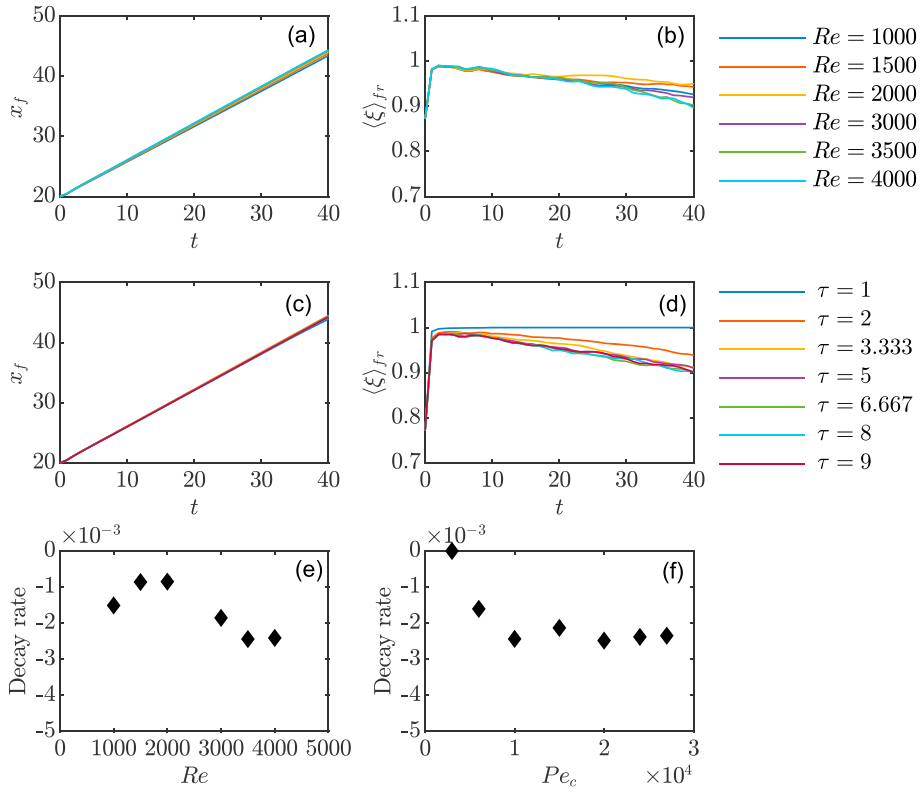

Figure 3. (a) Dependence of front location x_f on Re (Pe_c! = 40,000 and Pe_s = 4,000). (b) Dependence of freshness-to-sediment ratio $\langle\xi\rangle_{fr}$ on Re (Pe_c = 40,000 and Pe_s = 4,000). (c) Dependence of front location x_f on Pe_c (Re = 3,000 and Pe_s = 3,000). (d) Dependence of freshness-to-sediment ratio $\langle\xi\rangle_{fr}$ on Pe_c (Re = 3,000 and Pe_s = 3,000). (e) Decay rate of the freshness-to-sediment ratio $\langle\xi\rangle_{fr}$ (calculated by $\frac{\langle\xi\rangle_{fr,\ t=40} - \langle\xi\rangle_{fr,\ t=10}}{30}$) as function of Re. (f) Decay rate of the freshness-to-sediment ratio $\langle\xi\rangle_{fr}$ as function of Pe_c .

All frames of Figure 2 show the development of a bottom-propagating current with a pronounced head and an upper interface that gives rise to large-scale Kelvin-Helmholtz instabilities. For $\tau = 1$ we find that the sediment concentration and the freshness have identical distributions, consistent with our earlier arguments. Consequently, the freshness-to-sediment ratio $\xi = 1$ where sediment is present, which means that the current gains salinity at the same rate as it loses sediment. For $\tau = 8$, on the other hand, the current gains salinity much more rapidly than it loses sediment. Hence, for $\tau = 8$ the increasing salinification of the current due to the differential diffusivities of salt and sediment progresses *without corresponding dilution of the sediment concentration field*. This is in contrast to salinification of the current by entrainment, that is, convective engulfment of salty ambient water without sediment, which necessarily dilutes the sediment concentration field.

The above observations are consistent with the *cs*-fields shown in Figure 2c. For $\tau = 8$ these demonstrate the much faster formation of salty, sediment-laden fluid near the current front and in the interfacial region along the top of the current, as compared to $\tau = 1$. In line with the arguments presented in section 3, the top frame in Figure 2d confirms that for $\tau = 1$ the values of the sediment concentration c and the freshness $(1 - s)$ of the fluid are identical everywhere, so that $\xi = (1 - s)/c$ equals one where sediment is present. For $\tau = 8$, on the other hand, the frontal region of the current shows reduced values of ξ, which indicates that the freshness of the current is reduced as a result of salinity diffusion into the current.

In addition to the immediate effect of rendering the interstitial fluid more saline, the diffusion of salt into the current triggers secondary mechanisms of importance for the dynamics of the current. For example, the diffusion of salt into the hyperpycnal current across its upper interface results in the formation of a dense, salty layer of sediment-laden fluid along the upper current boundary, above the lighter sediment-laden freshwater body of the current. This configuration is susceptible to smaller-scale density-driven instabilities (Alsinan et al., 2017; Burns & Meiburg, 2015; Schulte et al., 2016), which in turn will increase the entrainment of ambient

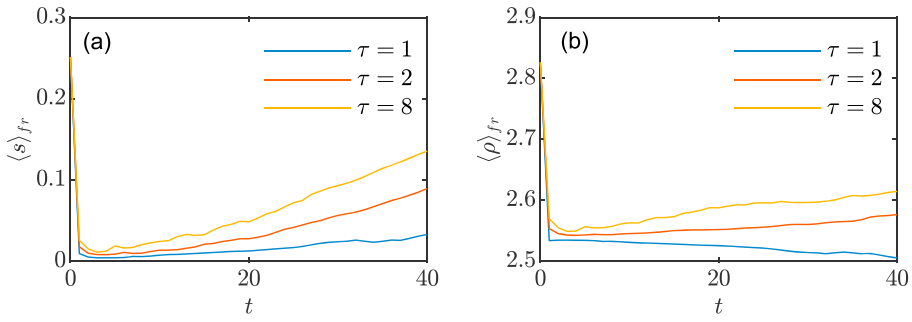

Figure 4. Average salinity (a) and density (b) in the frontal region of the current, where the sediment concentration $c > 0.9$. The large initial values represent an artifact, as no well-developed front has formed yet. Differential diffusivity is seen to increase the density of the frontal region of the current.

saline fluid into the current. The presence of these smaller-scale features is quite noticeable in the frames of Figure 2 for $\tau = 8$.

5. Estimating the Transition Time and Distance

Figures 3a and 3c demonstrate that the dimensionless front velocity is close to 0.5, and essentially independent of *Re* and Pe_c within the parameter ranges considered here. Figures 3b and 3d show that the freshness-to-sediment ratio $\langle \xi \rangle_{fr}$ decreases with time at a nearly constant rate, confirming that the freshwater hyperpycnal current is becoming increasingly saline. The results indicate that for $Pe_s = 4{,}000$, $Pe_c = 40{,}000$, and small Reynolds numbers, the decay rate of the ratio $\langle \xi \rangle_{fr}$, defined as the slope of the curve, grows with *Re*, which reflects the increasing turbulence intensity. For $Re = 3{,}000$ and $Pe_s = 3{,}000$ the decay rate no longer depends on Pe_c above $Pe_c = 10{,}000$. These observations are confirmed by Figures 3e and 3f, which indicate asymptotic decay rates for $\langle \xi \rangle_{fr}$ in the range of 2.5×10^{-3}. Extrapolating these results linearly to larger times suggests that for the model laboratory-scale currents with $Re = 3{,}000$ and large molecular diffusivities considered here, around $t \approx 200$ the value of $\langle \xi \rangle_{fr}$ will have decreased to about one half, which we can take as indication that the hyperpycnal flow has transitioned to a saline turbidity current. Since the dimensionless front velocity is close to 0.5, the hyperpycnal flow corresponding to the present parameter values thus has to travel approximately 100 current heights before it has transitioned into a saline turbidity current.

Alternatively, we can estimate the transition time by tracking the average salinity value in the front region as a function of time, as shown in Figure 4a. Extrapolating the results for $\tau = 8$ to longer times again suggests that for the laboratory-scale current with large molecular diffusivities considered here the averaged salinity value will reach one half after $t \approx 150-200$, consistent with the above estimate based on the freshness-to-sediment ratio. Figure 4b shows that differential diffusion increases the average density in the frontal region of the gravity current, thereby promoting longer runout distances.

6. Discussion

The above simulations demonstrate that differential diffusivities can provide a mechanism for hyperpycnal flows to transition into saline turbidity currents. In contrast to transition via ambient saltwater entrainment, transition by differential diffusivities does not require diluting the sediment concentration field. While the present simulations were carried out in two dimensions, and for laboratory-scale *Re*- and *Pe*-values much smaller than those encountered in large-scale geophysical flows, the physical mechanisms observed here should qualitatively apply also at those much larger scales. Translating the present scaling results regarding transition time and distance to field scales is not straightforward, as the larger *Re*-values combined with three-dimensional effects will modify the turbulence structure, and real molecular diffusivities will be much smaller. At the same time, we need to keep in mind that in natural settings the available distance over which the transition can occur may be 10^3 to 10^4 current heights, (e.g., Gavey et al., 2017; Meiburg & Kneller, 2010). Hence, the current investigation represents a first step that will hopefully motivate future experimental and computational studies at larger field scales, in order to explore the influence of vigorous, shear-induced turbulence at the interface, along with double-diffusive convection at realistic values of the molecular diffusivity.

7. Conclusion

We have provided a new perspective on the transition of hyperpycnal flows into saline turbidity currents, which suppresses their lofting and contributing to longer runout lengths. This mechanism, which relies on the differential diffusion of salt and sediment, results in the salinification of the freshwater current without diluting the sediment concentration field. We propose the freshness-to-sediment ratio in order to quantify the transition process. High-resolution simulations suggest that laboratory-scale hyperpycnal model flows with enhanced molecular diffusivities can transition into saline turbidity currents after traveling a few hundred current heights. Further research is needed in order to obtain estimates for the transition time and length at field scales and realistic molecular diffusivities.

Acknowledgments
E.M. gratefully acknowledges support through NSF grant CBET-1438052. L.Z. thanks The National Natural Science Foundation of China (11672267) and the China Scholarship Council for providing him with a scholarship to study at UCSB. B.V. was supported by a Feodor-Lynen scholarship from the Alexander von Humboldt Foundation, Germany. Computational resources for this work were made available by the Extreme Science and Engineering Discovery Environment (XSEDE), which is supported by NSF grant TGCTS150053. All of the data employed in this work can be obtained at https://drive.google.com/drive/folders/1pfg-sBgZeXcu3GbbrOa62FX87qcozzyl?usp=sharing.

References

Alsinan, A., Meiburg, E., & Garaud, P. (2017). A settling-driven instability in two-component, stably stratified fluids. *Journal of Fluid Mechanics*, *816*, 243–267.

Biegert, E., Vowinckel, B., & Meiburg, E. (2017). A collision model for grain-resolving simulations of flows over dense, mobile, polydisperse granular sediment beds. *Journal of Computational Physics*, *340*, 105–127.

Biegert, E., Vowinckel, B., Ouillon, R., & Meiburg, E. (2017). High-resolution simulations of turbidity currents. *Progress in Earth and Planetary Science*, *4*(1), 33. https://doi.org/10.1186/s40645-017-0147-4

Blanchette, F., Strauss, M., Meiburg, E., Kneller, B., & Glinsky, M. E. (2005). High-resolution numerical simulations of resuspending gravity currents: Conditions for self-sustainment. *Journal of Geophysical Research*, *110*, C12022. https://doi.org/10.1029/2005JC002927

Burns, P., & Meiburg, E. (2015). Sediment-laden fresh water above salt water: Nonlinear simulations. *Journal of Fluid Mechanics*, *762*, 156–195.

Carter, L., Milliman, J. D., Talling, P. J., Gavey, R., & Wynn, R. B. (2012). Near-synchronous and delayed initiation of long run-out submarine sediment flows from a record-breaking river flood, offshore Taiwan. *Geophysical Research Letters*, *39*, L12603. https://doi.org/10.1029/2012GL051172

Davis, R. H. (1996). Hydrodynamic diffusion of suspended particles: A symposium. *Journal of Fluid Mechanics*, *310*, 325–335.

Gavey, R., Carter, L., Liu, J. T., Talling, P. J., Hsu, R., Pope, E., & Evans, G. (2017). Frequent sediment density flows during 2006 to 2015, triggered by competing seismic and weather events: Observations from subsea cable breaks off southern Taiwan. *Marine Geology*, *384*, 147–158.

Gladstone, C., & Pritchard, D. (2010). Patterns of deposition from experimental turbidity currents with reversing buoyancy. *Sedimentology*, *57*(1), 53–84.

Hebert, D., & Ruddick, B. R. (2003). Differential mixing by breaking internal waves. *Geophysical Research Letters*, *30*(2), 1042. https://doi.org/10.1029/2002GL016250

Hu, P., Pähtz, T., & He, Z. (2015). Is it appropriate to model turbidity currents with the three-equation model? *Journal of Geophysical Research: Earth Surface*, *120*, 1153–1170. https://doi.org/10.1002/2015JF003474

Kneller, B., Nasr-Azadani, M. M., Radhakrishnan, S., & Meiburg, E. (2016). Long-range sediment transport in the world's oceans by stably stratified turbidity currents. *Journal of Geophysical Research: Oceans*, *121*, 8608–8620. https://doi.org/10.1002/2016JC011978

Konopliv, N., & Meiburg, E. (2016). Double-diffusive lock-exchange gravity currents. *Journal of Fluid Mechanics*, *797*, 729–764.

Luchi, R., Balachandar, S., Seminara, G., & Parker, G. (2018). Turbidity currents with equilibrium basal driving layers: A mechanism for long runout. *Geophysical Research Letters*, *45*, 1518–1526. https://doi.org/10.1002/2017GL075608

McCave, I. N., & Jones, K. P. N. (1988). Deposition of ungraded muds from high-density non-turbulent turbidity currents. *Nature*, *333*(6170), 250–252.

McDougall, T. J. (1985). A model of a frictionless double-diffusive gravity current on a horizontal surface. *Geophysical & Astrophysical Fluid Dynamics*, *31*(3-4), 221–245.

Meiburg, E., & Kneller, B. (2010). Turbidity currents and their deposits. *Annual Review of Fluid Mechanics*, *42*, 135–156.

Merryfield, W. J. (2005). Dependence of differential mixing on N and Rρ. *Journal of Physical Oceanography*, *35*(6), 991–1003.

Mulder, T., & Alexander, J. (2001). The physical character of subaqueous sedimentary density flows and their deposits. *Sedimentology*, *48*(2), 269–299.

Mulder, T., & Syvitski, J. P. M. (1995). Turbidity currents generated at river mouths during exceptional discharges to the world oceans. *The Journal of Geology*, *103*(3), 285–299.

Mulder, T., Syvitski, J. P. M., Migeon, S., Faugeres, J.-C., & Savoye, B. (2003). Marine hyperpycnal flows: Initiation, behavior and related deposits. A review. *Marine and Petroleum Geology*, *20*(6-8), 861–882.

Nakajima, T. (2006). Hyperpycnites deposited 700 km away from river mouths in the central Japan Sea. *Journal of Sedimentary Research*, *76*(1), 60–73.

Necker, F., Härtel, C., Kleiser, L., & Meiburg, E. (2002). High-resolution simulations of particle-driven gravity currents. *International Journal of Multiphase Flow*, *28*(2), 279–300.

Parker, G., Fukushima, Y., & Pantin, H. M. (1986). Self-accelerating turbidity currents. *Journal of Fluid Mechanics*, *171*, 145–181.

Schulte, B., Konopliv, N., & Meiburg, E. (2016). Clear salt water above sediment-laden fresh water: Interfacial instabilities. *Physical Review Fluids*, *1*(1), 012301.

Segre, P. N., Liu, F., Umbanhowar, P., & Weitz, D. A. (2001). An effective gravitational temperature for sedimentation. *Nature*, *409*(6820), 594.

Smyth, W. D., Nash, J. D., & Moum, J. N. (2005). Differential diffusion in breaking Kelvin-Helmholtz billows. *Journal of Physical Oceanography*, *35*(6), 1004–1022.

Sparks, R. S. J., Bonnecaze, R. T., Huppert, H. E., Lister, J. R., Hallworth, M. A., Mader, H., & Phillips, J. (1993). Sediment-laden gravity currents with reversing buoyancy. *Earth and Planetary Science Letters*, *114*(2-3), 243–257.

Steel, E., Buttles, J., Simms, A. R., Mohrig, D., & Meiburg, E. (2017). The role of buoyancy reversal in turbidite deposition and submarine fan geometry. *Geology*, *45*(1), 35–38.

Sutherland, B. R., Gingras, M. K., Knudson, C., Steverango, L., & Surma, C. (2018). Particle-bearing currents in uniform density and two-layer fluids. *Physical Review Fluids*, *3*(2), 023801.

Talling, P. J. (2014). On the triggers, resulting flow types and frequencies of subaqueous sediment density flows in different settings. *Marine Geology*, *352*, 155–182.

Talling, P. J., Masson, D. G., Sumner, E. J., & Malgesini, G. (2012). Subaqueous sediment density flows: Depositional processes and deposit types. *Sedimentology*, *59*(7), 1937–2003.

Talling, P. J., Paull, C. K., & Piper, D. J. W. (2013). How are subaqueous sediment density flows triggered, what is their internal structure and how does it evolve? Direct observations from monitoring of active flows. *Earth-Science Reviews*, *125*, 244–287.